

Antenna Pointing Accuracy Impact on Geostationary Satellite Link Quality and Interference

Ralph Brooker*

RBrooker Engineering, 422 N. Alfred St, Alexandria, VA, 22314, USA.

Dan Vorderbrueggen†

Andrew Corporation, 2601 Telecom Parkway, Richardson, TX, USA.

In an environment of mass-market direct-to-home and broadband services provided by closely spaced Ka-band satellites, cost pressures drive antenna diameters down until adjacent satellite rejection limits are reached. At the same time, antenna mount costs are being reduced and allocated alignment time per antenna is now measured in minutes. These factors combine to make antenna pointing error a potentially significant contributor to interference and link degradation. Pointing errors can be categorized as static or dynamic. Static errors, which are defined as the error after installation, include CP squint and mount mechanism tolerance effects such as lock-down shift, backlash, and mechanical-to-optical axis misalignment. Dynamic errors may be long term, such as foundation settling, spacecraft stationkeeping, and differential heating, or short term, such as wind deflection. Computation of the net pointing vector error must take into account factors external to the antenna, such as signal meter noise and integration time, signal fluctuation due to propagation, and most important, the procedural sequence followed by the installer, such as the simple peak method or the bracketing method. Many of these error contributors have systematic and random components. We have used numerical simulation methods, with graphic illustrations, to evaluate the statistical pointing error behavior of typical low-cost Ku- and Ka-band antennas in conjunction with practical pointing procedures and installer equipment. Probability distributions of pointing loss and adjacent satellite interference ratio are found. For multi-feed antennas the effect of skew misalignment is explored, and the tradeoffs between el-over-az vs. polar and quasi-polar mount geometries are analyzed. Simulation results show that mechanical accuracy specifications must be defined in conjunction with defined alignment procedures and installer equipment characteristics in order to constrain pointing loss and interference. The simulation method also offers techniques for effectively training installers by graphically illustrating the effect of adjustments and mount characteristics as the alignment process is rehearsed.

Nomenclature

<i>CP</i>	= circular polarization
θ	= off-axis angle
θ_3	= off-axis angle at the -3dB relative gain point
G_r	= antenna gain relative to on-axis gain (dB)
EIRP	= Effective Isotropic Radiated Power
QPSK	= Quadrature Phase Shift Keying
VSAT	= Very Small Aperture Terminal

* Principal

† Senior Systems Engineer, Earth Station Antenna Systems

I. Introduction

SHARING of the geostationary arc necessitates antennas with beamwidths much less than the orbital spacing. The consequences of mispointing are gradual: as Fig. 1 illustrates, antenna gain away from boresight falls off continuously. If the antenna is mispointed, link margin to the target satellite is degraded. Further, gain in the direction of an adjacent satellite can increase, causing signals from those satellites to interfere with the intended downlink, or in the case of an uplinking station, to create excess interference.

Pointing error (in terms of angle and loss) is comprised of a static component, due to imperfect aiming at the time of installation, and dynamic components, which vary over time. The pointing error combined with uplink signal characteristics determines the level of off-axis radiated power. As Fig. 2 suggests, many contributing factors combine in a manner which is made complex by the algorithmic nature of the pointing procedure, which in turn depends on operator skill and training, and by the random nature of many of the error factors.

In this study, numerical simulation techniques combine behavioral modeling of the antenna mechanism with the human installer's procedure, signal-measuring instrument properties, antenna patterns, and link analyses to predict statistical pointing performance of typical small earth stations.

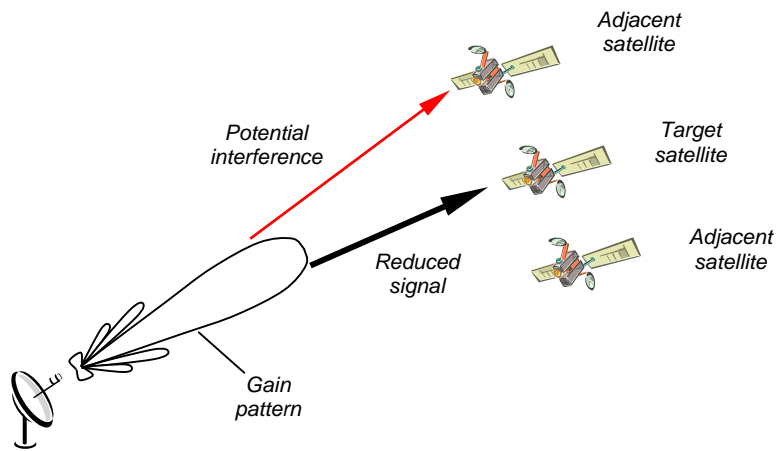


Figure 1. Earth station mispointing effects.

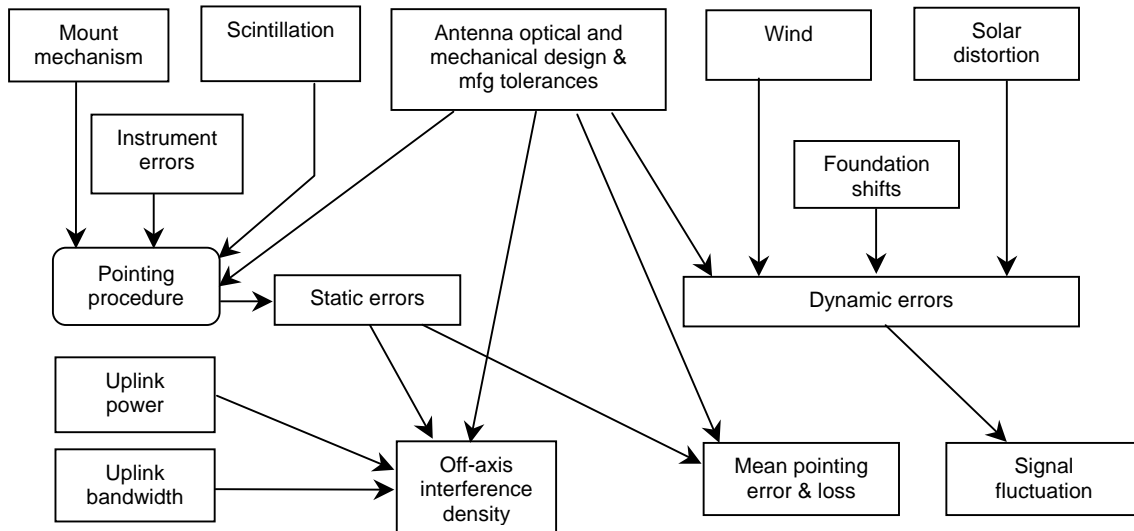


Figure 2. Contributions to pointing error.

II. Categorization of errors

A. Mechanical and optical error sources

A fixed antenna mount may be reasonably well characterized by its ideal design parameters and a set of static and dynamic error characteristics, described as follows.

1. Pointing adjustment mechanism characteristics

Antenna mount mechanisms have mechanical adjustment behaviors that can be described by the following set of parameters, illustrated in Figs. 3 and 4:

(i) *Adjustment resolution* is defined as the minimum antenna beam movement in azimuth or elevation that can be effected with the corresponding actuator. It represents the granularity of motion.

(ii) *Sensitivity* is defined as the change in beam direction per unit of actuator adjustment. If the actuator were, for example, a bolt head, the sensitivity would be in units of degrees/turn.

(iii) *Hysteresis span* is defined as the difference in actual beam direction for a given actuator setting position after being approached from two opposite directions. Hysteresis, also known as backlash, can be caused by bearing slack, imperfect thread fit, etc.

(iv) *Hysteresis repeatability* is defined as the difference in actual beam direction for a given reference actuator setting position, after traversing the hysteresis span and approaching from the same direction. Hysteresis span and repeatability are shown in Fig. 3 for a forward-backward-forward maneuver.

(v) *Lock-down shift*, illustrated in Fig. 4, is defined as the azimuth-elevation vector change when the locking fasteners are tightened after all final adjustments have been made. It is comprised of a systematic component, which may vary from one antenna to the next, and a random component, which varies each time the locking fasteners are tightened.

2. Antenna design and tolerance characteristics

Manufacturing tolerances and design criteria cause certain unchanging, or static, pointing error contributions:

(i) *Absolute azimuth and elevation errors* are defined as the difference between the scale or instrument readings and the absolute values of azimuth and elevation. They are commonly due to compass and inclinometer accuracy limitations and manufacturing tolerances of the scale markings.

(ii) *Boresight-axis misalignment* applies to asymmetric antennas and is defined as the angular difference between the optical boresight and the skew axis of rotation. It can be caused by a variety of factors, including reflector shape error, tolerance in the mounting points of the reflector, and feed position error.

(iii) *Polarization and tilt setting accuracy* is defined as the difference between the polarization scale reading and the actual plane of polarization of the signal. Causes include manufacturing tolerance of the feed arm, internal symmetry of the feed horn and polarizer waveguide, and scale placement accuracy.

(iv) *Vertical plumb error* is defined as the difference between the azimuth axis of rotation and the local vertical and is generally caused by the foundation or base pole being imperfectly leveled. Plumb error in the east-west direction (for a south-pointing antenna) adds to polarization and tilt error, whereas plumb error in the north-south direction adds to absolute elevation error.

(v) *Beam squint*, in circularly polarized antennas, is defined as plus and minus half of the difference between the LHCP and RHCP main beam directions. It occurs in single-reflector offset-fed paraboloidal antennas when the feed horn is aimed towards the center of the reflector rather than along the paraboloid axis.¹ The squint angle is on the

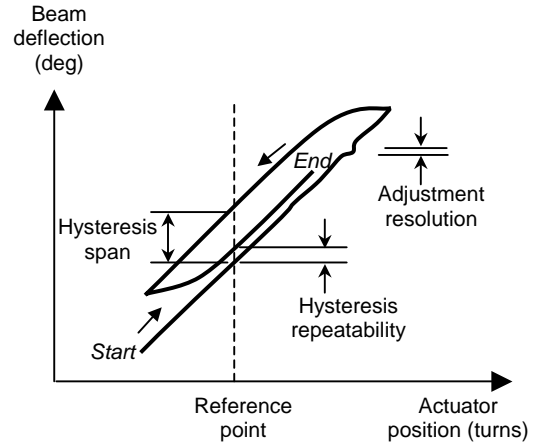


Figure 3. Hysteresis behavior.

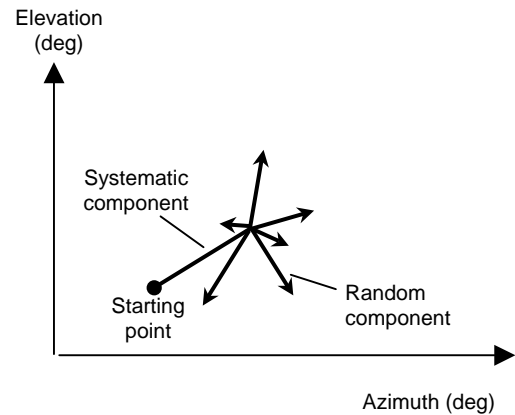


Figure 4. Lock-down shift behavior.

order of $\pm 0.15^\circ$ for a sub-meter antenna at 12 GHz; it increases with the tilt angle of the feed from the axis and is approximately inversely proportional to frequency and focal length.

3. Dynamic errors

Unlike the above static errors, sources of dynamic error vary over time. They include:

(i) *Wind deflection.* The primary tradeoff for antenna structural design is very often stiffness against reflector wind load versus cost, weight, and complexity. Wind deflection has stochastic temporal behavior; wind resistance of a reflector antenna is strongly dependent on the angle of arrival of the wind, which varies over time, and the wind velocity has a random spectrum generally containing a slow-changing “steady” component and faster-changing “gust” components. This spectrum interacts with the stiffness transient and resonant response of the structure.

(ii) *Uneven solar heating of the reflector.* At sunrise and sunset, the shadow of the edge of a large reflector may take a significant time to traverse the width of the reflector. During this period, the sunlit portion of the reflector dissipates greater solar heat load than the shadowed portion, which can result in shape distortion due to differential expansion. The first order effect is a shift in boresight direction with no indication from axis sensors.

(iii) *Foundation settling* is defined as change vertical plumb error over time, due to ground or structural settling.

(iv) *Station keeping* is defined as motion of the satellite with respect to the earth.

B. Instrumentation error sources

Manual and most automatic peaking procedures employ measurements of the magnitude of received signals and assume that indicated signal level varies only with antenna pointing loss. Several factors introduce randomness which, to a degree that depends on the procedure, violate that assumption and degrade pointing accuracy:

1. Meter resolution

In low-cost wide-band IF meters, resolution is manifested as step size (for digital-display meters), meter needle size and scale (for analog meters), or perceptible pitch or beep-rate change (for tone meters). For this class of meters resolution is typically on the order of 0.1-0.3 dB.

2. Noise in measurement bandwidth

Satellite signal spectra have power spectral densities similar to band-limited Gaussian noise. Therefore the indicated level of one signal, or a set of signals, will have a random component that is a function of the detector bandwidth. Example simulations of the standard deviation of the reading for meters reading in both decibels and in Watts as a function of the post-detection time constant are shown in Fig. 5, for various pre-detection bandwidths.

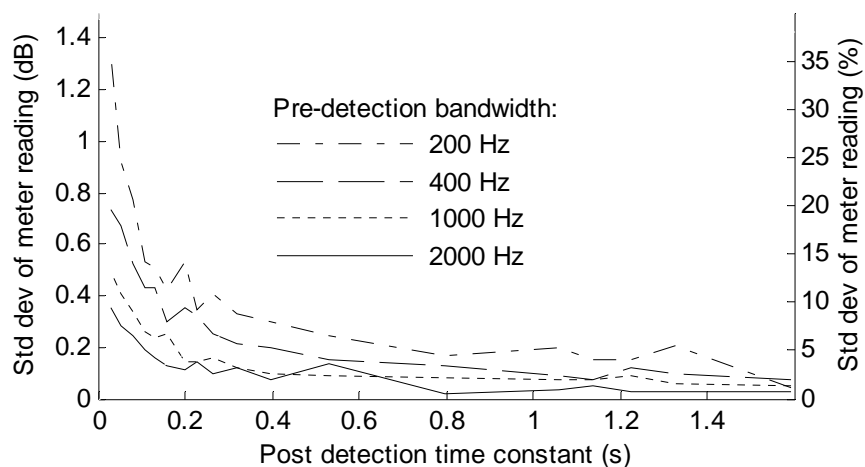


Figure 5. Standard deviation of signal meters measuring noise-like signals.

3. Scintillation

Turbulent irregularities in atmospheric temperature, humidity, and pressure create small-scale, moving variations in refractive index.² In otherwise steady state conditions, this time-varying multipath adds Gaussian noise to signal level measurements.³ A typical measurement sequence, taken from NASA ACTS experiment data at 20 GHz) is shown in Fig. 6. The standard deviation of the induced noise in the readings is highly dependent on humidity, but can be on the order of 0.1 – 0.25 dB at Ka-band or .06 – .19 dB RMS at Ku-band (assuming 1 sample per second).

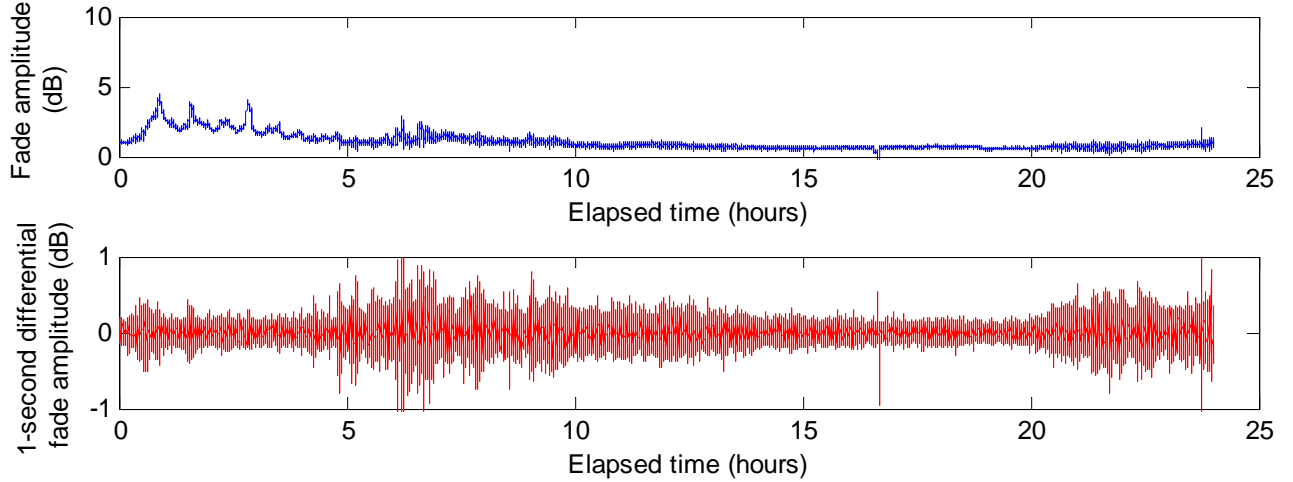


Figure 6. Sample data from the NASA ACTS experiment (20 GHz).

4. Fade drift

As Fig. 6 also illustrates, longer-term changes in path loss occasionally occur, primarily due to rain events, but also from cloud cover changes, fog, and antenna/feed wetting and drying. Since most peaking techniques assume consistency over 10-60 seconds in order to compare signal readings at different pointing settings, drift in readings within this time scale can shift the perceived optimum pointing settings.

C. Procedural error factors

1. Simple peak method

The simplest method for pointing an antenna is to adjust for maximum receive strength of an independent signal (e.g. beacon). As Fig. 7 illustrates, the pointing error due to instrument level measurement error can be derived from the assumption that the main lobe of the antenna is approximately parabolic:

$$G_r(\theta) = 3 \left(\frac{\theta}{\theta_3} \right)^2$$

The pointing error angle is thus

$$\theta_{err} = \theta_3 \sqrt{\frac{2E}{3}}$$

where the error level measurement during the course of the peaking maneuver is $\pm E$ dB.

A variation on this method is to maximize the strength of a signal transmitted from the same antenna. In this case the receive and transmit antenna patterns multiply, giving an effectively narrower beam. The pointing error angle is then:

$$\theta_{err} = \sqrt{\frac{\theta_{3R}^2 \cdot \theta_{3T}^2}{\theta_{3R}^2 + \theta_{3T}^2}} \cdot \sqrt{\frac{2E}{3}}$$

where θ_{3R} and θ_{3T} are the receive and transmit 3-dB half beamwidths, respectively.

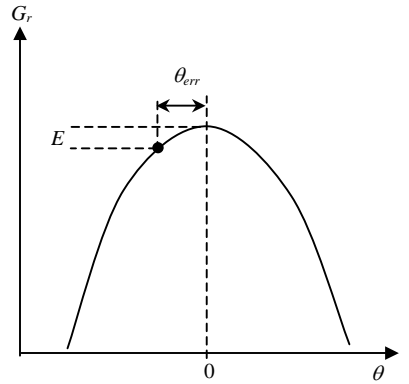


Figure 7. Simple peak pointing method.

2. Beam bracketing method

If the pointing adjustment mechanism affords a reasonably consistent indication of antenna deflection angle, the beam bracketing method may be used to take advantage of the steep and symmetric slopes of the antenna beam shoulders. One basic form of this method is as follows (refer to Fig. 8):

- Step 1: Find the peak and note the level;
- Step 2: Move to an arbitrary loss point L dB down from the peak on one side and note the actuator position as the zero mark;
- Step 3: Move to the same loss point on the other side of the beam noting the new actuator position a ;
- Step 4: Set the actuator to the position halfway between the two noted positions $a/2$.

With this method the worst case pointing error due to level measurement error E is:

$$\theta_{err} = \frac{\theta_3}{2\sqrt{3}} \left(\sqrt{L+E} - \sqrt{L-E} \right)$$

Figure 9 shows the pointing losses and error angles for 100 trials using methods described above, applied to a 0.75m, 65%-efficient antenna at 14 GHz transmit and 11.7 GHz receive, with measurement tolerance $E = \pm 0.2$ dB and using a bracketing level $L = 3$ dB. Note that using even such a moderate bracketing level improves the pointing error angle by an order of magnitude, leaving lock-down shift and other errors more likely to dominate.

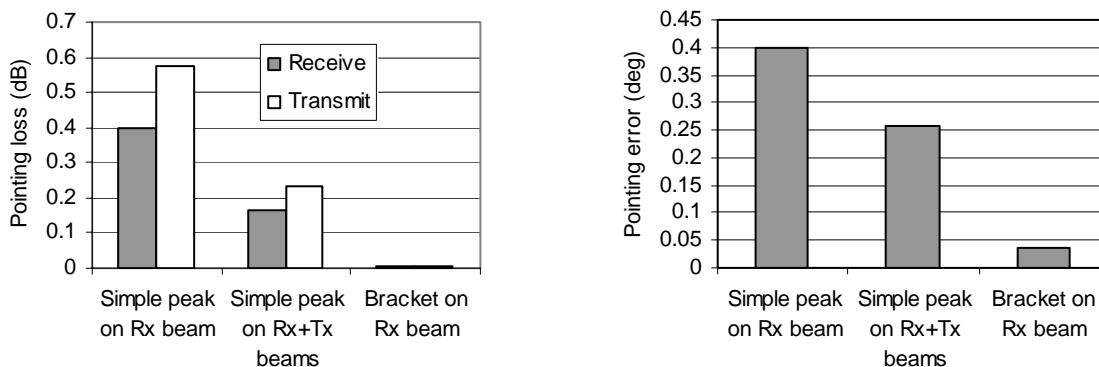


Figure 9. Comparison of pointing methods for a 0.75m Ku-band antenna.

3. Cross-pol method

Single-reflector offset antennas have a boresight null but high “rabbit ears” in the cross-pol gain patterns, as exemplified by Fig. 10. The peaks of the “ears” occur at approximately the angle of -6 dB co-pol gain⁴ and their height varies in the range -30 to -20 dB below maximum co-pol gain, depending on focal length and offset angle. The deep and narrow null allows cross-pol signal strength ratio to be used both as a sensitive indication of pointing accuracy and as an indication of polarization adjustment accuracy. Note, however, that null depth can be limited by polarizer performance, and further, due to feed symmetry tolerances, that the null may not be exactly centered on the co-pol beam shoulders.

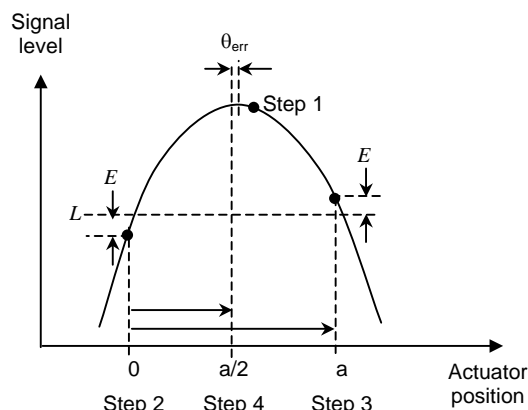


Figure 8. Beam bracketing pointing method.

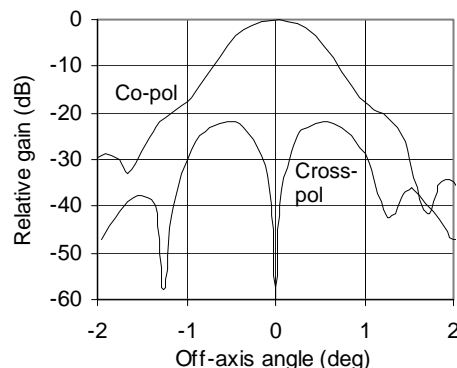


Figure 10. Example offset reflector antenna patterns.

III. Simulation examples

Because the antenna pattern, pointing procedure, and mount mechanical characteristics combine in a complex manner, numerical simulation is a useful tool to quickly predict the pointing accuracy of large populations of terminals. For this purpose a Matlab-based pointing vector and link simulation engine was developed that computes the vectors of the antenna beam(s) and the vectors to the satellite in the frame of reference of the station site, using the method of rotation and translation of frames of reference from the center of the earth to the site location and through all pivot axes on the mount and antenna, including tolerances. From these vectors pointing error angles are computed, which are then mapped to the modeled gain patterns of the antenna to determine pointing losses and uplink EIRPs in the direction of the adjacent satellites. A link computation is made and readings on spectrum analyzers and wideband signal meters are emulated.

The simulator presents a graphical user interface for manual emulation of the pointing process (a feature that is also useful for training, as discussed in Section IV), and controls for automatic randomized repetition and accumulation of results, from which statistical case studies can be made. The following examples illustrate the utility of this technique for various applications.

A. Multi-beam Ku-band RO antenna across wide orbit position span

Multibeam antennas pose a challenge to installers because the tilt (skew) angle must be aligned accurately, in addition to azimuth and elevation. A hypothetical example is for a Ku-band receive only antenna with the main beam receiving a satellite at 100°W and a scanned (side-offset feed) beam receiving a satellite at 118°W. The view from Los Angeles of these satellites, as well as of other satellites spaced at 4.5° intervals, is shown in Fig. 11. Also overlaid are the 0.5-dB and 25-dB gain contours of the main and scanned beam of an imperfectly-pointed antenna, which in this case is modeled as an elliptical 0.75 m-equivalent reflector.

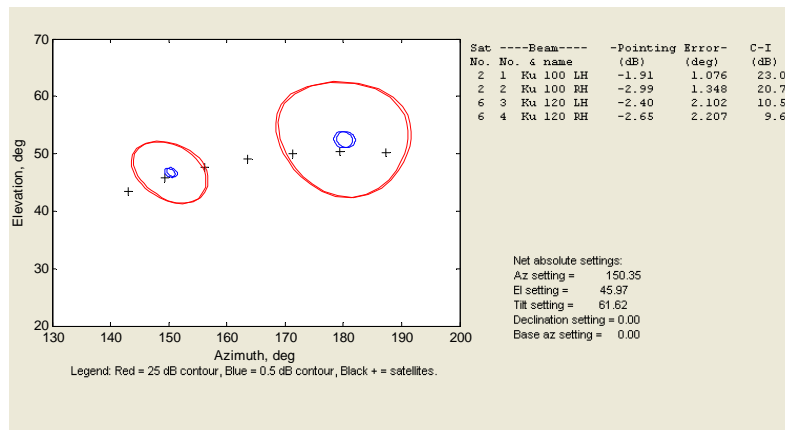


Figure 11. Sky view of an example dual-beam, dual-satellite scenario.

The pointing simulation model accounts for random mount errors, including +/- 0.05° lock down shifts, +/- 0.5° pole plumb error, +/- 1° skew setting accuracy, and other mechanical factors. The results 100 trial simulations using simple peaking are shown in Fig. 12. Note that the main beam mean loss is non-zero, due to the simple peaking algorithm which terminates when the signal reading (with random fluctuations and meter rounding) is within a tolerance factor of one meter step (0.2 dB) of the highest value observed when passing through beam center. The scanned beam loss, however, is often closer to zero, because the skew angle is randomized and the designed beam scan angle is necessarily a compromise for all geographical locations at which the terminal may be placed.

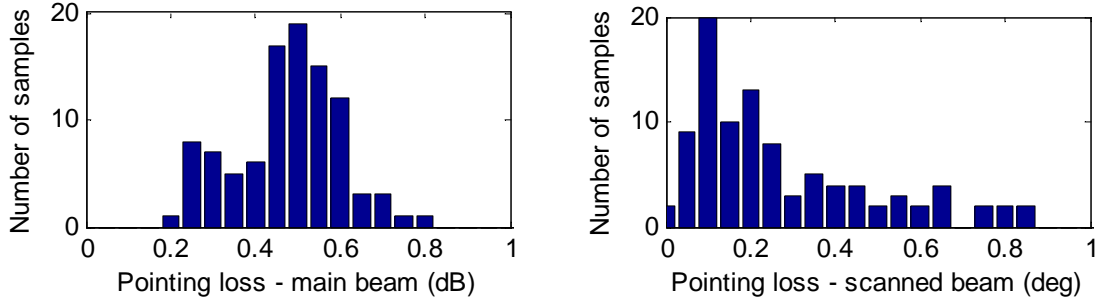


Figure 12. Pointing statistics using simple peaking.

The above example illustrates the sensitivity of pointing accuracy to installer skill. Results of the same simulation repeated with the beam bracketing method on the main beam, shown in Fig. 13, indicate that this method is substantially more accurate and consistent. Note that peaking is on the main beam only and that skew is simply preset to the nominal value for the site.

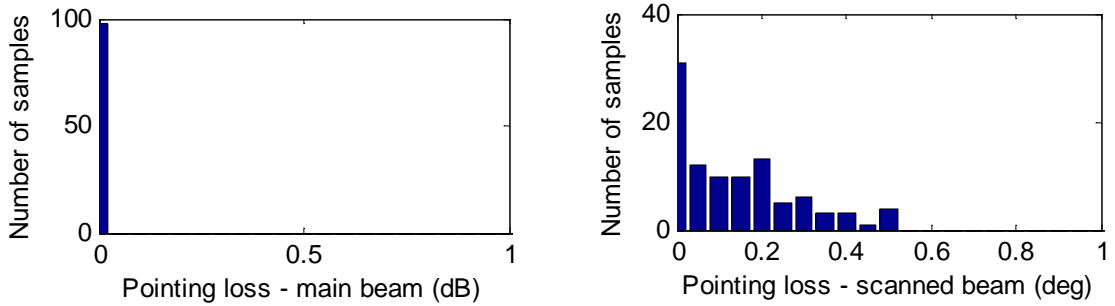


Figure 13. Pointing statistics using beam bracket peaking.

B. Ka/Ku Satellite Interactive Terminal (SIT)

SIT systems using 30 GHz uplink and 12 GHz downlink beams represent a particularly difficult pointing challenge. As the 100-trial simulation results in Fig. 14 show, because the Ka-band uplink beam is much narrower, a simple peaking on the Ku-band downlink beam can result in extremely poor uplink pointing loss. Beam bracketing offers a substantial improvement, as illustrated in Fig. 15, but can still be impacted by CP beam squint. In this example the uplink and downlink beams are assumed to be both circularly polarized and on opposite polarizations, resulting in about 0.25 degrees divergence between the beams due to squint.

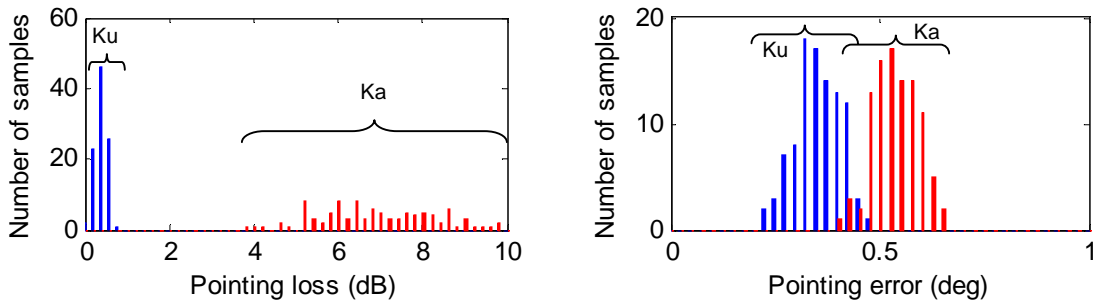


Figure 14. Pointing statistics using simple peaking.

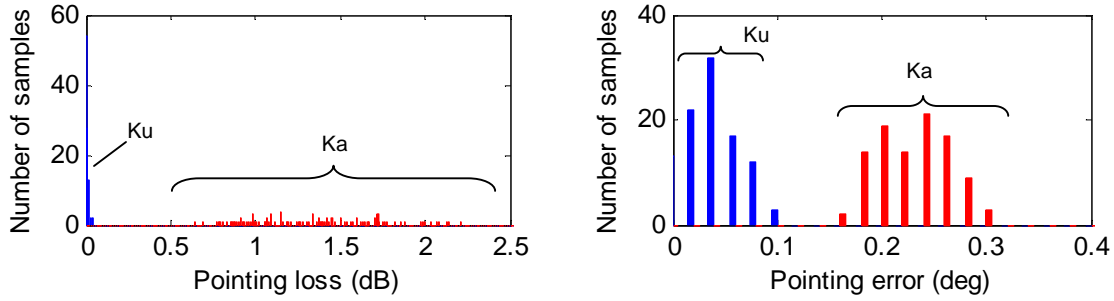


Figure 15. Pointing statistics using beam bracket peaking.

C. Adjacent-Satellite Interference at 2-degree spacing from a Ku-band VSAT uplink

Ku-band VSATs are typically pointed using the received hub signal and are locked down prior to enabling of the uplink. If pointing is not accurate and not independently checked (e.g. using the cross-pol null method), the pointing error can result in unacceptable EIRP spectral density radiated towards adjacent satellites. To examine this effect and its sensitivity to antenna diameter, simulations were made for a hypothetical uplink from a VSAT with three alternative dish sizes (75cm, 96cm, and 120cm) and both simple and beam bracketing pointing methods.

Statistics for pointing error angle for a 100-trial simulation are shown in Fig. 16. The heavy line represents the range of results, and the intermediate cross markers represent one standard deviation below mean, the mean, and one standard deviation above mean, respectively. The left figure shows pointing error angle and illustrates the dominance of lock-down shifts errors when peaking accurately with the bracketing method. The right figure shows adjacent satellite interference in terms of worst-case EIRP spectral density towards satellites at orbit locations +/- 2° from the target satellite. Here, the assumed signal has a total EIRP of 39 dBW and bandwidth equivalent to 256 kbps QPSK with rate 1/2 coding.

This simulation illustrates the importance of caution and coordination when deploying sub-meter Ku-band VSATs.

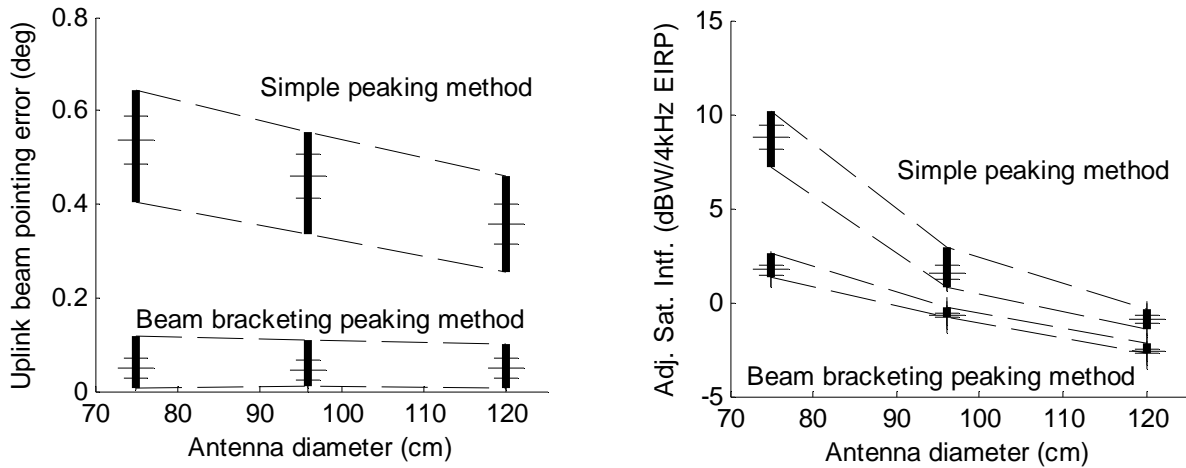


Figure 16. Ku VSAT pointing error and adjacent satellite interference levels.

D. C-band 4.9m antenna with 2-degree satellite spacing

Because beamwidth increases with wavelength, C-band antennas in the 2.4-5m range also require particular care with pointing. Taking the case of the Andrew 4.9 m antenna as an example, the error parameters of the mount (such as lockdown shift and hysteresis) are negligible, so the static pointing errors are dominated by signal measurement accuracy, as Fig. 17 illustrates. Use of the beam bracketing method, by contrast, results in the very accurate performance shown in Fig. 18. A by-product of the antenna's high-gain, symmetric dual-reflector optics is a first sidelobe level that intersects the $29-25\log(\theta)$ regulatory reference curve (Fig. 19). Nevertheless, pointing accuracy simulation shows that the gain remains below the reference curve under worst case pointing errors at the closest angle at which a 2-degree-spaced satellite can appear, i.e., $\pm 2.08^\circ$ for 10° elevation.

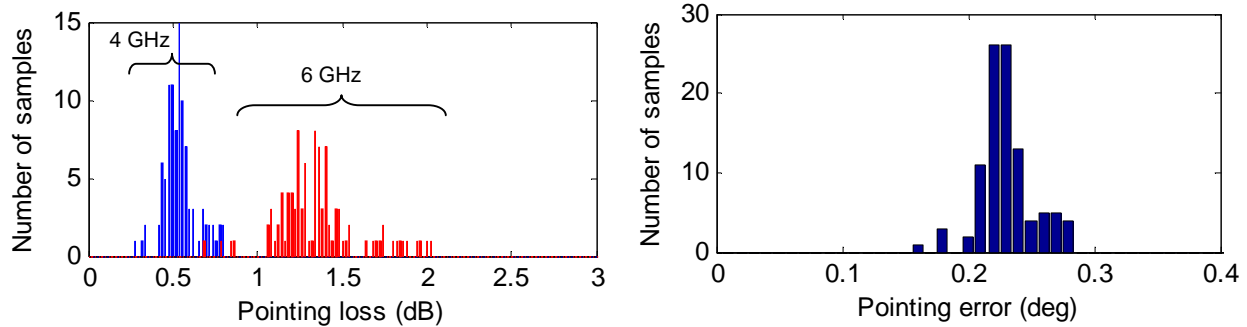


Figure 17. Pointing statistics using simple peaking.

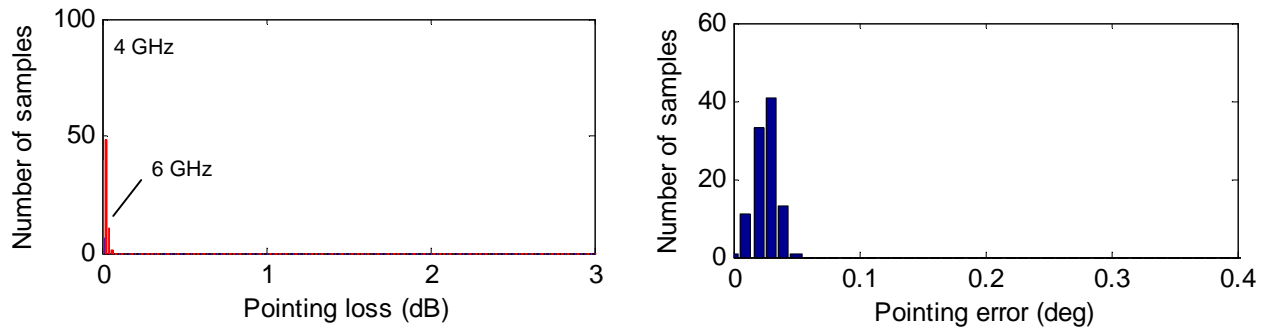


Figure 18. Pointing statistics using beam bracket peaking.

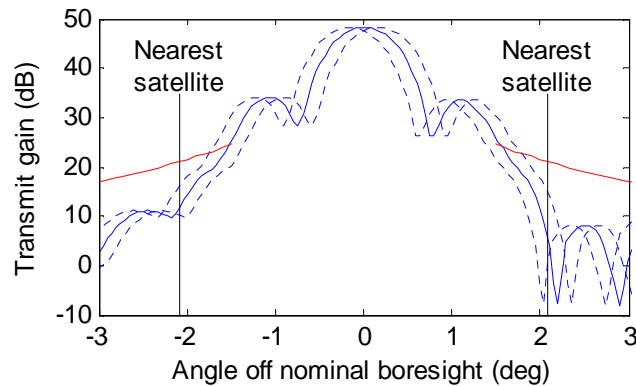


Figure 19. Andrew 4.9m antenna, transmit beam.

Solid line represents typical antenna gain pattern. Dashed lines represent the extents of antenna beam deflection under worst-case pointing error (using beam bracket method) and wind gusting. Limit lines represent the $29 - 25\log(\theta)$ curve, beginning at 1.5° per FCC regulation 25.209, pending revision⁵.

IV. Training Applications

Numerical simulation of the mechanical behavior of the antenna mount, coupled with pattern emulation and link computation and presented with graphical user interfaces that mimic the installer-operated controls, can make a powerful training tool for installer skills practice. An example of a prototype user interface is shown in Fig. 20. Here, the student installer can manipulate the coarse and fine azimuth, elevation, and lock down mechanisms on a modeled antenna, while at the same time monitoring meters that emulate the behavior of standard field instruments including scintillation effects.

To help the student visualize the overlay of antenna beams and satellites, a separate “sky view” screen (shown previously in Fig. 11) is coupled to the controls. Once the student achieves a sense of the effects of the control input actions, the sky view can be closed, and the student may practice operating on “instruments only.”

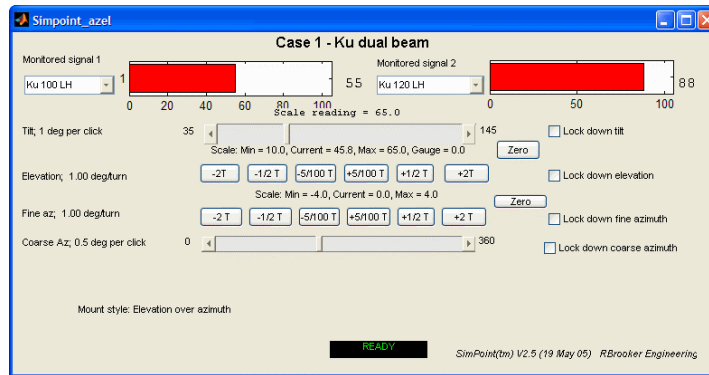


Figure 20. Training application user interface screen.

V. Conclusions

Numerical simulation is a powerful tool for predicting the statistical performance of realistic antenna mechanisms used in practical pointing procedures. Sample results highlight the importance of installer technique for repeatable and accurate pointing, and especially of the value of the beam-bracketing method as opposed to simple peaking based in signal strength. The simulation technique enables antenna manufacturers to rationally optimize mount mechanical performance and to define the corresponding installation procedures required to achieve overall link performance and interference mitigation objectives in a large population of VSAT or direct-to-home receive terminals.

Acknowledgments

The authors wish to acknowledge the support of Andrew Corporation for this study.

References

- ¹ Duan, D.-W. and Rahmat-Samii, Y., “Beam Squint Determination in Conic-Section Reflector Antennas with Circularly Polarized Feeds,” *IEEE Trans. Ant. Prop.*, Vol. 39, No. 5, May 1991, pp. 612-619.
- ² van de Kamp, M. M. J. L., Riva, C., Tervonen, J. K., and Salonen, E. T., “Frequency Dependence of Amplitude Scintillation,” *IEEE Trans. Ant. Prop.*, Vol. 47, No. 1, Jan 1999, pp. 77-85.
- ³ Catalan, C., Gyemont, B., and Vilar, E., “Frequency Scaling Factor of Amplitude Scintillation Variance for Satellite Communication Systems,” *National Conference on Antennas and Propagation*, 30 March - 1 April 1999, IEE Conference Publication No. 461.
- ⁴ Knop, C., “Microwave-Relay Antennas,” *Antenna Engineering Handbook*, 3rd ed., edited by R. C. Johnson, McGraw Hill, New York, 1993, p. 30-20.
- ⁵ Federal Communications Commission, Sixth Report and Order and Third Further Notice of Proposed Rulemaking, FCC 05-62, International Bureau Docket no. 00-248, March 15, 2005.